Electronic Supplementary Information (ESI)

# Synthesis of Cu₂SnSe₃-Au heteronanostructures with optoelectronic and photocatalytic properties

Wenliang Wang,[abcd] Tao Ding,[abcd] Guihuan Chen,[abcd] Li Zhang,[abcd] Yongqiang Yu[abce] and Qing Yang*[abcd]

[a]Hefei National Laboratory of Physical Sciences at the Microscale (HFNL), University of Science and Technology of China (USTC), Hefei 230026, Anhui, P. R. China. E-mail: qyoung@ustc.edu.cn; Fax: +86-551-63606266; Tel: +86-551-63600243.

[b]Department of Chemistry, USTC, Hefei 230026, Anhui, P. R. China.

[c]Laboratory of Nanomaterials for Energy Conversion (LNEC), USTC, Hefei 230026, Anhui, P. R. China.

[d]Synergetic Innovation Center of Quantum Information & Quantum Physics, USTC, Hefei 230026, Anhui, P. R. China.

[e]School of Materials Science and Engineering, Hefei University of Technology, Hefei 230009, Anhui, P. R. China.

## Experimental Section

**Materials.** Triphenyltin chloride ($Ph_3SnCl$, 95%), dibenzyl diselenide (($PhCH_2)_2Se_2$, 95%), 3-mercaptopropionic acid (MPA, 99%) and octadecene (ODE, 98%) were purchased from Alfa Aesar. Oleylamine (OAm, 70%) was purchased from Aldrich. Anhydrous copper chloride (CuCl), chloroauric acid tetrahydrate ($AuCl_3 \cdot HCl \cdot 4H_2O$), methylene blue (MB), absolute ethanol, ethylene glycol and toluene were obtained from Sinopharm Chemical Reagent Ltd., China. All chemicals were used directly without any purification.

**Preparation of Stock Solution.** Gold stock solution was prepared by dissolving 1.0 g of $AuCl_3 \cdot HCl \cdot 4H_2O$ in 100 mL distilled water.

**Synthesis of CTSe Nanocrystals.** Quasi-spherical CTSe nanoparticles with cubic structure were prepared by the reaction of copper, tin salts with dibenzyl diselenide in the presence of OAm and ODE. In a typical synthesis, stoichiometric amounts of CuCl (0.2 mmoL) and $Ph_3SnCl$ (0.1 mmoL) in the presence of OAm (2.0 mL) and ODE (3.0 mL) were added in a three-neck flask. The solution was magnetically stirred and heated to 180 °C for 30 min under an argon atmosphere to remove water and other low-boiling point impurities. At the same time, ($PhCH_2)_2Se_2$ (0.15 mmoL) was dissolved in 1.0 mL OAm in a vial, which was preheated to 70 °C. After that, the Cu

(I) and Sn (IV) complexes were heated to 280 °C. Then the Se-OAm solution was immediately injected into the above solution and the reaction mixture was kept at 280 °C for 5 minutes with continuous stirring. The reaction was allowed to cool to room temperature naturally. Finally, the product was collected by centrifugation and washed several times with absolute ethanol and toluene. The product obtained in this case was cubic phase CTSe nanoparticles with monodisperse and uniform size (see Fig. S1).

**Ligand Exchange.** The above obtained CTSe NCs were added to 1.0 mL of MPA and 5.0 mL toluene mixture in a 10 mL beaker after ultrasonication for 15 min and allowed to stand overnight at room temperature, to replace the weakly bound OAm. Finally, the sample was collected by centrifugation and washed several times with absolute ethanol and toluene. The ligand bound to the surface of the CTSe NCs was analyzed by ATR-FTIR spectroscopic technique (see Fig. S2).

**Synthesis of CTSe-Au Heteronanostructures.** In a typical synthesis, the ligand-exchanged CTSe nanocrystals were dispersed in 15 mL ethylene glycol and 1.0 mL OAm under ultrasonication and magnetic stirring. Then 2.0 mL gold stock solution was added drop-wise under stirring to the above CTSe nanocrystals solution at room temperature. After stirring for about 20 min, the product was immediately precipitated by adding absolute ethanol with centrifugation and washed several times with absolute ethanol and toluene, respectively. Finally, the obtained CTSe-Au nanocrystals were dispersed in toluene for further characterization. As can be seen in Fig. S4, the size of attached Au nanoparticles on CTSe nanocrystals was around 4.6 nm.

**Characterization.** The samples were characterized by X-ray power diffraction (XRD), using a Philips X'Pert PRO SUPER X-ray diffractometer equipped with graphite monochromaticized Cu Kα radiation ($\lambda$ = 1.54056 Å). The operation voltage and current were kept at 40 kV and 400 mA, respectively. Transmission electron microscopy (TEM), high-resolution transmission electron microscopy (HRTEM), and the corresponding selected-area electron diffraction (SAED) were performed on Hitachi H-7650 and JEOL 2010 with an acceleration voltage of 200 kV, respectively. The compositions of the samples were investigated by energy dispersive X-ray spectroscopy (EDX, OXFORD INCA system), high-angle annular dark-field imaging in the scanning TEM (HAADF-STEM), and electron energy loss spectroscopy (EELS). X-ray photoelectron spectroscopy (XPS) was acquired on an ESCALAB MK II with Mg Kα as the excitation source. The surface structures of the samples were determined by attenuated total reflection Fourier transformed infrared (ATR-FTIR) spectroscopy (Prestige-21, SHIMADZU). Optical absorption spectra were recorded on a spectrophotometer (DUV−3700 UV−vis-NIR) from 300 to 1350 nm at room temperature. Inductively coupled plasma atomic emission spectroscopy (ICP-AES) analysis performed on PerkinElmer Model Optima 3000DV was used to quantify the composition of the NCs. Optoelectronic characteristics of the devices were recorded with a two-probe method using an electrochemical station (CHI660e) and xenon lamp (PLS-SXE300) was selected as a white light source in a shielded and clean box at room temperature.
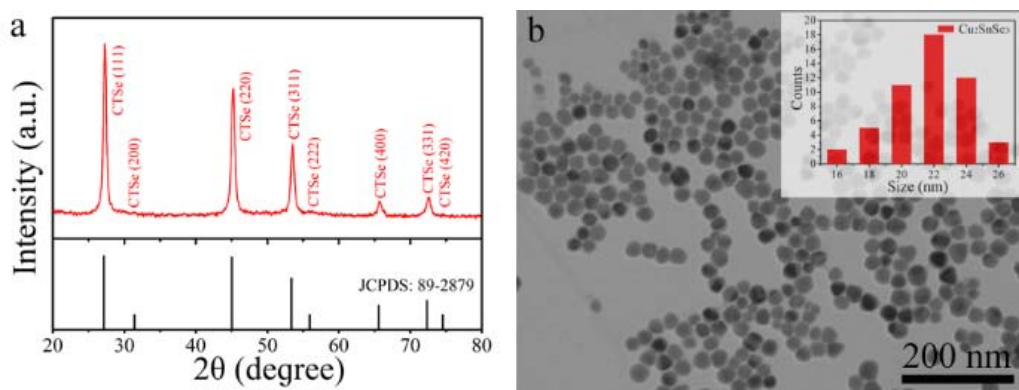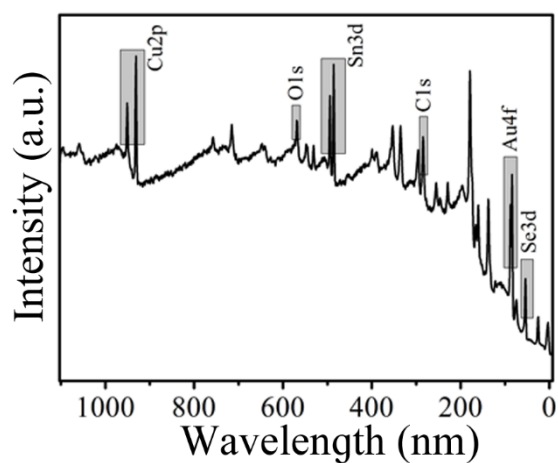
**Fig. S1** (a) XRD pattern, and (b) TEM image with the corresponding size-distribution histogram (inset) of the as-synthesized CTSe NCs.
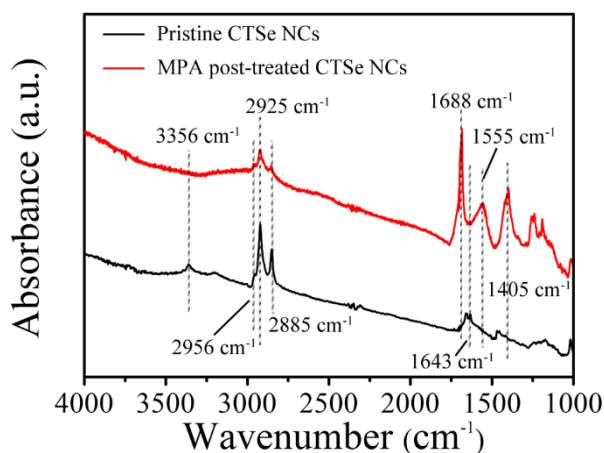


**Fig. S2** ATR-FTIR spectra of the as-synthesized CTSe NCs, black and red curves refer to the results of the CTSe samples before and after ligand exchange with MPA.

To examine the effectiveness of ligand-exchange method, ATR-FTIR was further employed to characterize the capping agents bound to the surface of the CTSe NCs. Fig. S2 shows the ATR-FTIR spectra of the CTSe NCs with OAm as the ligand (black line) and after ligand exchange with MPA (red line), respectively. The absorbance bands in the range of 2800-3000 cm$^{-1}$ can be assigned to the C-H stretching modes. The bands at 3356 and 1643 cm$^{-1}$ are attributed to N-H stretching and bending modes, respectively, revealing the presence of OAm on the particle surface (black line).[S1, S2] After ligand-exchange with MPA (red line), the peaks for N-H stretching and bending disappear, while three new bands at 1688, 1555 and 1405 cm$^{-1}$ are corresponding to C=O and COO$^-$ stretching modes,[S3] respectively, indicating the presence of acetate group attached to the CTSe NCs. These results demonstrate that the MPA becomes the main ligand bound to the CTSe NCs after ligand-exchange process.
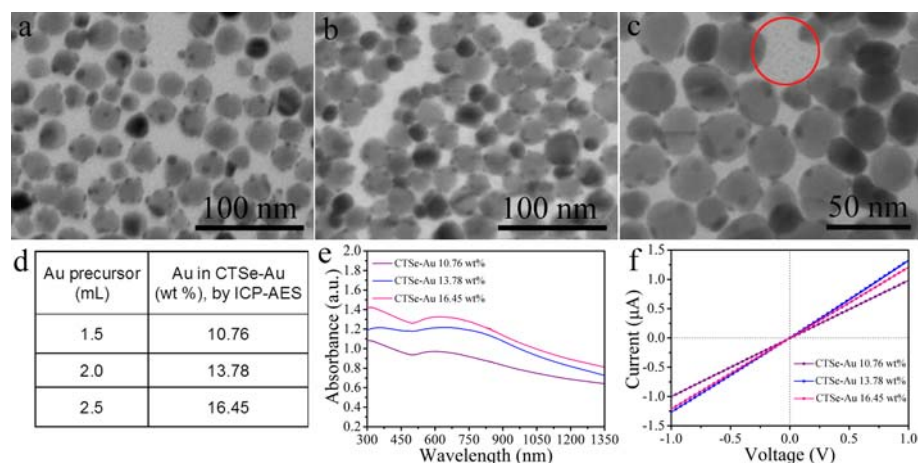
**Fig. S3** XPS survey spectrum of the as-synthesized CTSe-Au heteronanostructures.
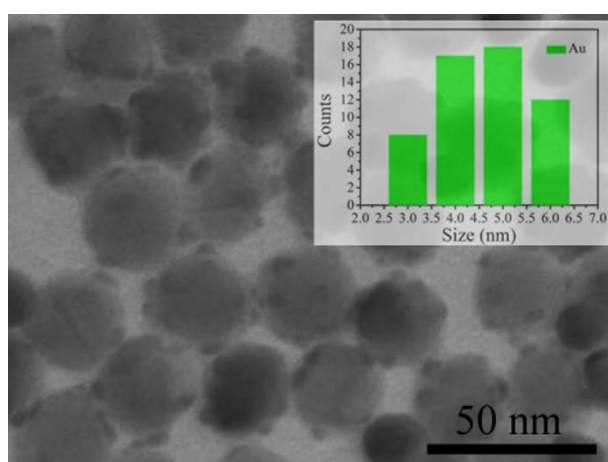


**Fig. S4** High-magnification TEM image of the as-synthesized CTSe-Au NCs and the corresponding size-distribution histogram (inset) of the Au nanoparticles.



| Element | Atomic % |
|---------|----------|
| Cu | 29.59 |
| Sn | 16.80 |
| Se | 47.43 |
| Au | 6.18 |
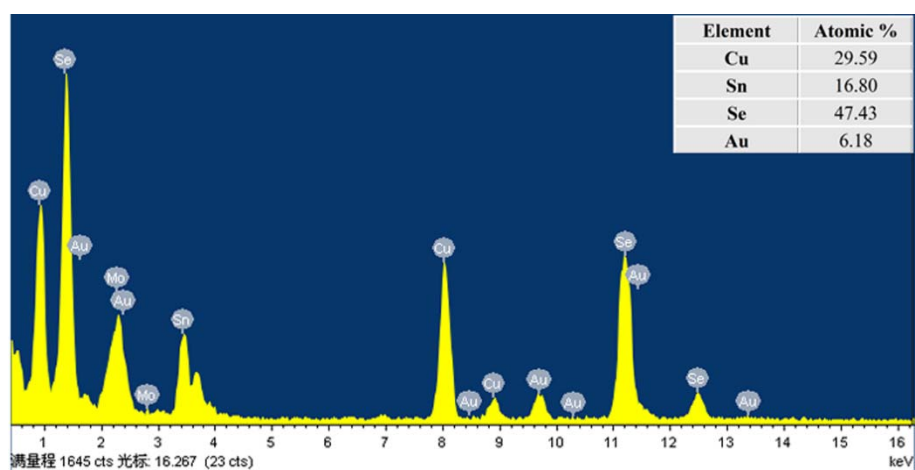
**Fig. S5** EDX spectrum of the as-synthesized CTSe-Au heteronanostructures.

**Fig. S6** (a-c) Typical TEM images of the as-synthesized CTSe-Au heteronanostructures with different volume addition ratios of Au precursor (a = 1.5 mL, b = 2.0 mL, c = 2.5 mL, the red circle inset of c showing the presence of independent Au NPs). (d) the corresponding loading content of Au (wt%) in the CTSe-Au heteronanostructures characterized by ICP-AES analysis, and (e) and (f) UV-vis-NIR absorption spectra and photocurrent of CTSe-Au heteronanostructures with different Au (wt%), respectively.

Currently, we have also studied the influence of different Au loading values on the optical and optoelectronic properties of the CTSe-Au heteronanostructures. Fig. S6a-c display the TEM images of the as-synthesized CTSe-Au heteronanostructures with different volume addition ratios of Au precursor. It is clearly observed that more Au NPs are loaded on the surfaces of the CTSe NCs with increased addition of Au precursor. Such results are good agreement with ICP-AES characterization (Fig. S6d). Fig. S6e shows the UV-vis-NIR absorption spectra of the CTSe-Au heteronanostructures with different weight ratios of Au NPs. It can be clearly observed for the series of the CTSe-Au heteronanostructures that the absorption intensity in the ranging from 400 to 800 nm is enhanced by the increase of the weight ratios of Au NPs. In general, the more loading of Au NPs leads to higher absorption of incident light,[S4, S5] which benefits the optoelectronic performance.[S6] However, excesses of Au NPs may attract holes and subsequently recombine them with electrons by acting as recombination centers to deteriorate the optoelectronic performance.[S4, S5, S7] A photodetector (the schematic of device configuration inset in Fig. 4c) is constructed by drop-casting concentrated toluene solution of the CTSe-Au NCs with different Au loading values on glass substrate and employed two adjacent ITO films as conductive electrodes. A xenon lamp equipped with a cut-off filter 400 nm is used as a white light source, which provides visible light ranging from 400 to 780 nm. As shown in Fig. S6f, the photocurrent increases with the Au load until a maximum at around 13.78 wt% and decreases with further Au loading. Compared to the Au content of 10.76 wt% in the CTSe-Au heteronanostructures, the improvement of photocurrent of the CTSe-Au heteronanostructures (Au load 13.78 wt%) is associated with the higher light absorption. However, the nucleation of independent Au NPs outside the CTSe surface occurs at too-high Au load (16.45 wt%, red circle in

Fig. S6c). Such independent Au NPs can act as recombination centers and lead to decrease the photocurrent. Thus, the above results confirm that appropriate band alignment and Au load content of the CTSe-Au heteronanostructures are considered as the important factors to faciliate solar energy conversion through an efficient charge separation and transfer of the photogenerated charge carriers from the semiconductor to the metal.
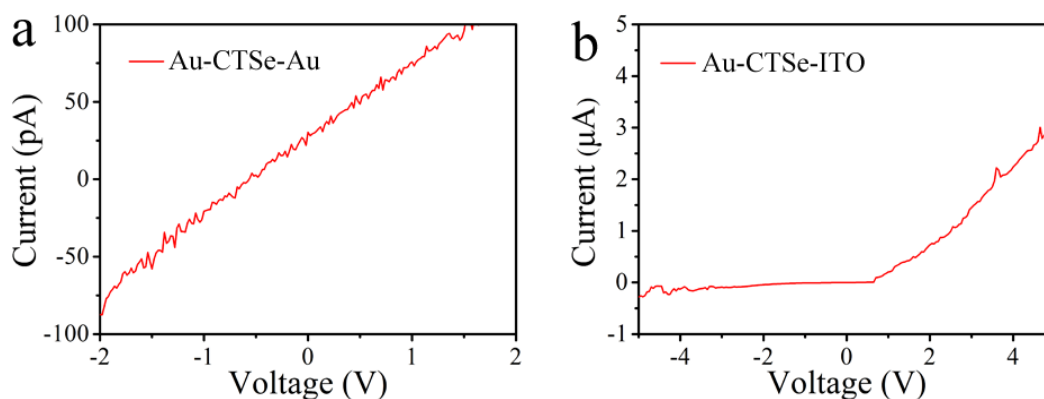


**Fig. S7** The I-V curves of the CTSe thin film based-device measured under different contact electrodes (a) Au-Au, and (b) Au-ITO.

Though it is difficult to determine the Schottky barrier height of an individual CTSe-Au heteronanostructure, an additional experiment is conducted to verify whether the existence of Schottky junction between CTSe and Au. To examine the contact effect, Au electrode is chosen as the contact electrode and deposited on CTSe thin film by sputtering method. As shown in Fig. S7a, Au-contact device exhibits very low conduction current ($\sim 10^{-11}$A at +1 V) as the noise level of our test system, indicating the contact resistance is so much higher than the values from using ITO contact electrode (Fig. 4). Such contact behavior could be proposed to be the Schottky contact. In order to further clarify our discussion, the current-voltage (I-V) is plotted in Fig. S7b by using Au and ITO electrodes as the contact electrode. Notably, the device shows a pronounced rectifying behavior, suggesting the existence of Schottky contact between Au and CTSe thin film.

## Estimation of the $E_g$, VB and CB edges of $Cu_2SnSe_3$

In the present work, the optical properties of the as-synthesized CTSe NCs dispersed in toluene are studied by UV−vis−NIR absorption spectroscopy (Fig. S8). The optical band gap is estimated by using a method based on the relation of $(\alpha h\nu)^n = A(h\nu − E_g)$, where $\alpha$ is the absorption coefficient, $h\nu$ is the photon energy, A is a constant, $E_g$ is the band gap energy, and n is 2 for a direct transition. Using this method, the optical band gap of CTSe NCs is estimated to be around 1.50 eV, which is close to the previous reports.[S8-S10] The conduction band-edge potential ($E_{CB}$) of a semiconductor can be calculated using the empirical equation: $E_{CB} = X_{comp} − E^e − 0.5E_g$,[S11-S13] $X_{comp}$ is the electronegativity of a compound which is given by the geometric mean of the electronegativities of the constituent atoms, $E^e$ is the energy of

free electrons on the hydrogen scale (i. e., $E^e$ = 4.5 eV), and $E_g$ is the band gap. In addition, the conduction band bottom ($E_{CB}$) can be determined by $E_{CB} = E_{VB} - E_g$. Thus, on the base of above equations, the $E_{VB}$ and $E_{CB}$ of the as-synthesized CTSe NCs are calculated to be about +1.35 and -0.15 eV with respect to the normal hydrogen electrode (NHE), respectively.
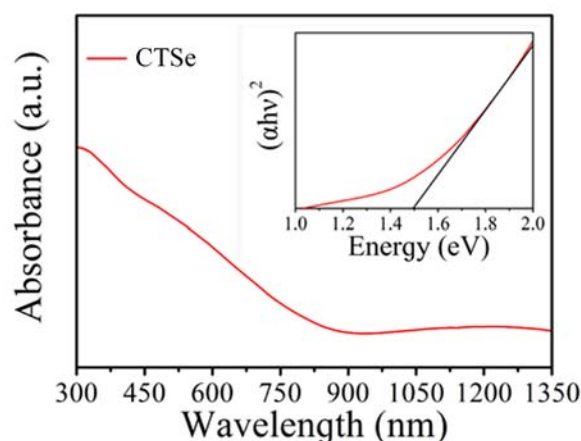


**Fig. S8** UV−vis−NIR absorption spectrum of the CTSe NCs, and the inset shows the band gap determined for these nanocrystals.

## Photocatalytic Measurements

For photocatalytic degradation of MB, the catalysts (50 mg, CTSe and CTSe-Au NCs) are added to the beaker containing 100 mL deionized water to be dispersed under ultrasonication, respectively. Then, MB 100 mL (10 mg/L) is added to above solution and the mixture is continuously stirred in dark for 30 min to achieve the dye absorption balance on the surface of catalysts. Subsequently, the photocatalytic test is conducted with stirring under visible light provided by a 300 W Xenon lamp (PLS-SXE300) equipped with a cut-off filter 400 nm, which provides visible light ranging from 400 to 780 nm. The sample compartment is water-cooled to eliminate the thermal effect during the photocatalytic reaction. The distance between the xenon light and the reaction solution is about 10 cm. The samples at certain time intervals are taken out and centrifuged for absorbance measurements using the spectrophotometer (DUV−3700 UV−vis-NIR). The concentration of MB is determined at its characteristic absorption wavelength of 664 nm. For comparison, the self-degradation of MB is also tested under same conditions in the absence of photocatalysts.

## Supplementary references

S1.     X. Lu, H.-Y. Tuan, J. Chen, Z.-Y. Li, B. A. Korgel and Y. Xia, *J. Am. Chem. Soc.,* 2007, **129**, 1733-1742.

S2.     W. Wang, J. Jiang, T. Ding, C. Wang, J. Zuo and Q. Yang, *ACS Appl. Mater. Interfaces,* 2015, **7**, 2235-2241.

S3.     X. Liu, X. Wang, B. Zhou, W. C. Law, A. N. Cartwright and M. T. Swihart,

*Adv. Funct. Mater.,* 2013, **23**, 1256-1264.

S4.     S. Han, L. Hu, N. Gao, A. A. Al‑Ghamdi and X. Fang, *Adv. Funct. Mater.,* 2014, **24**, 3725-3733.

S5.     S. Liu and Y.-J. Xu, *Nanoscale,* 2013, **5**, 9330-9339.

S6.     G. Manna, R. Bose and N. Pradhan, *Angew. Chem. Int. Ed.,* 2014, **53**, 6743-6746.

S7.     C. Wang, L. Yin, L. Zhang, N. Liu, N. Lun and Y. Qi, *ACS Appl. Mater. Interfaces,* 2010, **2**, 3373-3377.

S8.     M. Ahmadi, S. S. Pramana, S. K. Batabyal, C. Boothroyd, S. G. Mhaisalkar and Y. M. Lam, *Inorg. Chem.,* 2013, **52**, 1722-1728.

S9.     M. E. Norako, M. J. Greaney and R. L. Brutchey, *J. Am. Chem. Soc.,* 2012, **134**, 23-26.

S10.    J.-j. Wang, P. Liu, C. C. Seaton and K. M. Ryan, *J. Am. Chem. Soc.,* 2014, **136**, 7954-7960.

S11.    A. H. Nethercot Jr, *Phys. Rev. Lett.,* 1974, **33**, 1088.

S12.    Z. Lou, B. Huang, Z. Wang, X. Ma, R. Zhang, X. Zhang, X. Qin, Y. Dai and M.-H. Whangbo, *Chem. Mater.,* 2014, **26**, 3873-3875.

S13.    T. Cao, Y. Li, C. Wang, Z. Zhang, M. Zhang, C. Shao and Y. Liu, *J. Mater. Chem.,* 2011, **21**, 6922-6927.